In-Situ Monitoring of Electrooxidation Processes at a Gold Single Crystal Surface Using Shell-Isolated Nanoparticle-Enhanced Raman Spectroscopy

ARTICLE *in* JOURNAL OF THE AMERICAN CHEMICAL SOCIETY · JUNE 2015

Impact Factor: 12.11 · DOI: 10.1021/jacs.5b04670

JACS
JOURNAL OF THE AMERICAN CHEMICAL SOCIETY

Communication

pubs.acs.org/JACS

In Situ Monitoring of Electrooxidation Processes at a Gold Single Crystal Surface Using Shell-Isolated Nanoparticle-Enhanced Raman Spectroscopy

Chao-Yu Li,[†,#] Jin-Chao Dong,[†,#] Xi Jin,[†] Shu Chen,[‡] Rajapandiyan Panneerselvam,[†] Alexander V. Rudnev,[§] Zhi-Lin Yang,[‡] Jian-Feng Li,*[,†,§] Thomas Wandlowski,[§] and Zhong-Qun Tian[†]

[†]MOE Key Laboratory of Spectrochemical Analysis and Instrumentation, State Key Laboratory of Physical Chemistry of Solid Surfaces, College of Chemistry and Chemical Engineering, and [‡]Department of Physics, Xiamen University, Xiamen 361005, China

[§]Department of Chemistry and Biochemistry, University of Bern, Freiestrasse 3, Bern CH-3012, Switzerland

Supporting Information

ABSTRACT: Identifying the intermediate species in an electrocatalytic reaction can provide a great opportunity to understand the reaction mechanism and fabricate a better catalyst. However, the direct observation of intermediate species at a single crystal surface is a daunting challenge for spectroscopic techniques. In this work, electrochemical shell-isolated nanoparticle-enhanced Raman spectroscopy (EC-SHINERS) is utilized to in situ monitor the electrooxidation processes at atomically flat Au(*hkl*) single crystal electrode surfaces. We systematically explored the effects of crystallographic orientation, pH value, and anion on electrochemical behavior of intermediate (AuOH/AuO) species. The experimental results are well correlated with our periodic density functional theory calculations and corroborate the long-standing speculation based on theoretical calculations in previous electrochemical studies. The presented in situ electrochemical SHINERS technique offers a unique way for a real-time investigation of an electrocatalytic reaction pathway at various well-defined noble metal surfaces.

Clean energy, along with the booming economy and expanding population, has received great attention among the research community concerned with environmental issues. The fundamental understanding of the electrocatalytic process, the core of fuel cell and electrolysis, will be greatly beneficial to the fabrication of novel catalysts with high efficiency. There is a dearth of knowledge about electrocatalysis; the formation of an oxide film at a metal surface will decisively influence the activity of a catalyst and the reaction mechanism.[1] However, the process of surface electrooxidation is complicated, and the conventional characterization techniques for the identification of key intermediates, adsorbed oxygen species, or hydroxyl ions are still limited by the real-time performance and sensitivity.[2] It is noteworthy to mention that OH^- species play a key role in oxide film formation,[2] O_2 reduction,[1d,3] and electrooxidation of hydrogen.[4] Because of its importance, the oxidation of gold electrodes by means of electroreflectance spectroscopy was investigated by Nguyen et al.[5] Though the first direct evidence for the specific adsorption of OH^- on gold electrode was obtained, electroreflectance studies were unable to monitor the real-time oxidation process on an electrode surface. Therefore, it is imperative to investigate the adsorption behavior of hydroxide species on an electrode surface in a precise manner. Although various reaction mechanisms have been proposed based on electrochemical techniques and theoretical calculations, it is still a challenge to prove these results by direct evidence of in situ investigations at an atomically flat surface.[1d,2,6]

Surface-enhanced infrared reflection absorption spectroscopy (SEIRAS) is widely used in electrochemical interfaces investigation,[1b,7] but it is difficult to apply an IR technique at low wavenumbers below 800 cm^{-1}, where we can obtain the direct vibrational information on a molecule−metal bond, because of the absorption of infrared light by the thin solution layer and optical window. Surface-enhanced Raman spectroscopy[8] (SERS) is a unique analytical technique, which has been employed in electrochemical interface investigation,[9] monitoring reactions,[9c] biological analysis,[10] and other significant applications.[11] It inherits the advantage of acquiring Raman spectra and can obtain the bonding information at low wavenumbers without any interference from the ensemble. Notably, several efforts have been made using SERS to obtain the spectroscopic information on surface-oxygen species, unfortunately SERS is seriously limited to roughened nanostructured surfaces.[12] Particularly, single crystal surfaces are commonly preferred and used in surface science, because of their well-defined surface state and optic field. In addition, the information obtained from a single crystal surface will be greatly helpful to examine the orientation of adsorbates and to unravel the fundamental surface reactions unambiguously by using surface selection rules. In this contribution, tip-enhanced Raman spectroscopy[13] (TERS) and attenuated total reflection[14] (ATR) methods have been utilized to accrue spectral details at single crystal surfaces. Unfortunately, TERS was not able to be applied at electrochemical interfaces because of the interference from the tip immersed in solution and the low enhancement by only one tip so that only a few molecules could be used, whereas the latter technique is cumbersome and the enhancement factor (EF) is only 1 to 2 orders of magnitude. Therefore, a detailed description for the adsorption

Received: May 5, 2015

DOI: 10.1021/jacs.5b04670
J. Am. Chem. Soc. XXXX, XXX, XXX−XXX

behavior of an intermediate species such as the OH^- species at single crystal electrode surface remains elusive.

In 2010, our group invented a versatile tool called "shell-isolated nanoparticle-enhanced Raman spectroscopy" (SHINERS)[15] to open up new avenues in electrochemical interfaces, by resolving the disadvantages associated with TERS and ATR. Remarkably, shell-isolated nanoparticles (SHINs) render discernible Raman signals from single crystal surfaces with significant sensitivity, stability and reproducibility.[15,16] As a new technique, EC-SHINERS excels in the investigation of miscellany of adsorbates at single crystal surfaces and provides clear understanding about electrocatalytic processes.

Herein, we employ the in situ EC-SHINERS technique to monitor the surface oxidation processes at low-index Au(*hkl*) single crystal electrodes and systematically evaluate the influence of crystallographic orientation, anion, and pH during electrooxidation. Thus, the formation of hydroxide film is clearly elucidated with in situ EC-SHINERS.

Figure 1 manifests the process of in situ EC-SHINERS at low-index Au(*hkl*) surfaces. The SHINs utilized in this work

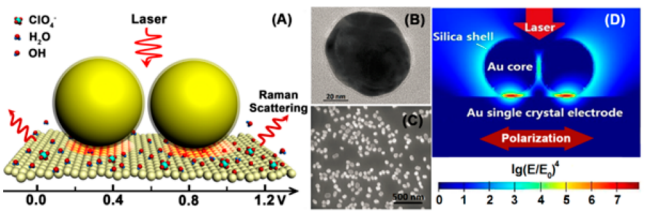

Figure 1. (A) Schematic diagram of in situ EC-SHINERS on low-index Au(*hkl*) surfaces. (B) HR-TEM image of Au@SiO_2 nanoparticle. (C) SEM image of Au(111) single crystal electrode surface modified with SHINs. (D) 3D-FDTD simulations of four SHIN NPs with a model of 2 × 2 array on an Au substrate.

consist of uniform Au nanoparticles (~55 nm) with a chemically grown SiO_2 shell (~2 nm). The size distribution of more than 100 SHINs is shown in Supporting Information, Figure S1. The as-prepared SHINs were carefully drop-casted onto a freshly prepared Au(*hkl*) single crystal half-bead electrode, and the electromagnetic simulations were performed using the finite-difference time-domain (FDTD) method. Four shell-isolated nanoparticles are placed on a gold single crystal substrate and illuminated using a linearly polarized plane wave with electric field amplitude of 1 V/m. As the electric field distribution shows (Figure 1D), the hot spots are located in the particle−film junctions under the 633 nm laser line. The modified electrode was subsequently mounted in a custom-made spectroelectrochemical cell.[16a,b] Pt and Ag/AgCl electrodes were used as counter and reference electrodes, respectively. After the modification of SHINs on the electrode surface, a hydrogen evolution reaction (HER) cleaning procedure is applied to remove the possible contamination. The electrochemical response of the modified single crystal surface is unaffected, which is evidenced by the cyclic voltammograms (CV).[16a] All potentials are reported with respect to Ag/AgCl electrode in this paper. The average enhancement factor of this configuration is about 1.1 × 10^6 on the Au(110) surface.[16b] Further details of the experiments can be found in the Supporting Information.

Figure 2 shows the CV of the Au(111) electrode in deaerated 0.1 M $NaClO_4$ solution (pH was tuned to ~9 with NaOH) at room temperature and corresponding in situ SHINERS spectra

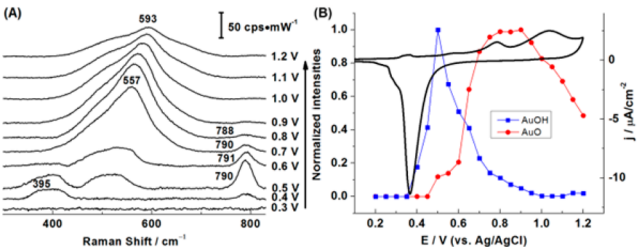

Figure 2. (A) In situ EC-SHINERS spectra of electrooxidation of the Au(111) surface in 0.1 M $NaClO_4$ (pH is ~9). (B) Normalized EC-SHINERS intensities of the stretching mode of AuO and the bending mode of AuOH at different potentials. CV of Au(111) electrode in 0.1 M $NaClO_4$ is presented (pH is ~9, scan rate is 2 mV/s).

during positive potential scan. During the positive potential excursion, there is no observable Raman signature in the range of 300 to 800 cm^{-1} until 0.4 V. However, at 0.4 V, a peak begins to appear around 790 cm^{-1} and the intensity reaches a maximum at ~0.5 V. On the basis of the periodic density functional theory (DFT) calculations on these three low index crystal surfaces, (as shown in the Supporting Information, Table S1 and Figure S6), and the literature data,[12a,d] we attribute this band to the gold-hydroxide bending mode δ_{AuOH} of the adsorption on top sites. Generally, hydroxide ions could specifically adsorb on the Au(111) surface and form $AuOH_{ad}$ through one-electron oxidation.[7,17] Importantly, at 0.5 V, the bending mode of AuOH is strongest which vividly emphasizes the maximum adsorption of the hydroxide ions on the Au(111) surface before their further oxidation to Au oxide. When the potential is higher, the oxidation and deprotonation of AuOH weakens the bending mode of AuOH (~790 cm^{-1}) which diminishes after complete oxidation of the Au (111) surface (>1.0 V). The peak slightly blue shifts from 790 to 791 cm^{-1} as potential increased from 0.5 to 0.6 V, and red shifts to 788 cm^{-1} as potential increased to 0.9 V. To ascertain our conclusion, a deuterium isotopic substitution measurement (as illustrated in Figure S2) was also carried out, and the bending mode of AuOH at 790 cm^{-1} shift toward the lower wavenumber 694 cm^{-1} in deuterated water was observed. This observation clearly implies that the band is attributed to the gold-hydroxide bending mode δ_{AuOH}, and accords well with the earlier reports on the roughened Au surface.[12d] In the low-frequency region, a broad band is present at ~360−420 cm^{-1} when the potential is set at 0.3 V. This band is ~20 cm^{-1} blue-shifted in deuterated water, which is similar to the experiments in previous publications, and it was assigned to Au−OH stretching.[12b,c]

Concurrently, at 0.5 V, a broad hump develops around 489−524 cm^{-1} which confirms the further oxidation of $AuOH_{ad}$ to AuO_{ad}.[7] This is also confirmed by our DFT calculation of the coadsorption model, as shown in Table S1 and Figure S7. Interestingly, the hump at higher wavenumber intensifies with increasing potential. At 0.7−1.2 V, the peak position shifts linearly from 557 to 593 cm^{-1}, and the intensity reaches a maximum at 0.8−0.9 V. It is evident that this potential-dependent behavior is derived from gold oxo-species at the electrode surface rather than that in the bulk. As demonstrated by Weaver's group, on the poly-gold electrode surface with ill-defined morphology,[12b,c] the band around 520−580 cm^{-1} is attributed to the AuO stretching mode. The frequency shift with electrochemical potential of the Au−O stretching mode is more significant than that of the bending mode. This may

DOI: 10.1021/jacs.5b04670
J. Am. Chem. Soc. XXXX, XXX, XXX−XXX

because of the dipole variation of the adsorbates during the Au−O stretching vibration which is parallel to the surface electric field.[18] Apparently, a decrement in Raman signal was observed with the growth of oxide film, because it weakens the electromagnetic coupling between the electrode surface and SHINs. Furthermore, the corresponding electro-reduction processes are followed as shown in Figure S3, and the reappearance of δ_{AuOH} peak is observed. During a negative scan, abundant surface oxide species at high potential were reduced to gold hydroxide gradually, which results in greater content of $AuOH_{ad}$ and thus stronger Raman intensity of δ_{AuOH} was observed.

Herein, the whole surface electrooxidation process at the atomically flat Au(111) surface as well as the potential dependent evolution of AuOH species have been in situ monitored using EC-SHINERS technique. These distinguishing spectral features corroborate the long-term speculation based on theoretical calculations in the electrochemical studies of oxidation intermediates.[2,6a,f,17,19]

To examine the effect of pH value on the formation of intermediate AuOH, we carried out controlled experiments with different pH values as well. As depicted in Figure 3, the

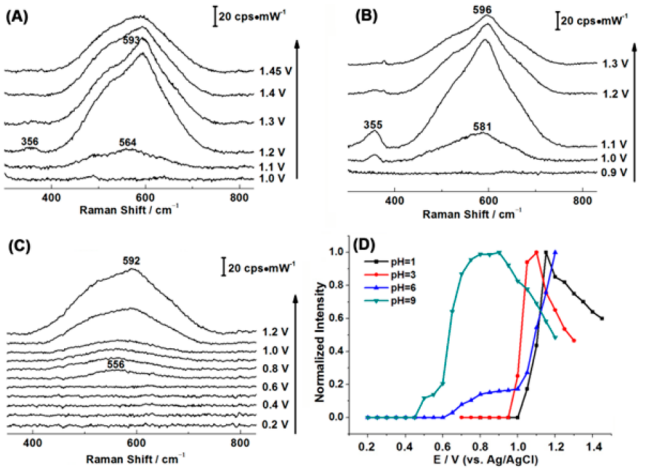

Figure 3. In situ EC-SHINERS spectra of electrooxidation of Au(111) surface during a positive scan in 0.1 M ClO_4^- solutions with different pH values. The pH values of the electrolytes in (A) 0.1 M $HClO_4$, (B) 0.1 M $NaClO_4$, and (C) 0.1 M $NaClO_4$ are 1, 3, and 6, respectively. (D) The related potential dependences of normalized Raman intensities for stretching mode of AuO in electrolytes with different pH values.

bending mode of AuOH is absent during the entire electrooxidation process when pH values are tuned to about 1, 3, and 6 (δ_{AuOH} mode at 796 cm^{-1} is observable in electrolyte with pH of 11, as shown in Figure S4). But the broad hump around 590 cm^{-1} remained in acid solution which confirms the contribution from the stretching mode of AuO. Apparently, the potential-dependent appearance of ν_{AuO} becomes lower with the increasing pH values, during the positive sweep (the potential-dependent appearance of ν_{AuO} in electrolytes with pH values of 1, 3, 6, 9, and 11 are 1.05, 1.0, 0.65, 0.5, and 0.3 V, respectively). This behavior clearly indicates that the onset of oxidation of the Au surface in basic solution is shifted to lower potential. Specifically, with the emergence of ν_{AuO} (potential is higher than 1.0 V), a band at ~355 cm^{-1} is present and the intensity decreases during extended surface oxidation. The Au−OH stretching mode located around 400 cm^{-1} is different from the broad band that appeared before the complete surface oxidation in basic solution. This narrow band (at ~355 cm^{-1}) could be assigned to bridging oxygen adsorption (Figure S7c).[12b] It is evidenced that the surface electro-oxidation mechanisms are rather different under different pH values.

Furthermore, to ascertain the role of anions, we performed the experiments in 0.1 M Na_2SO_4 solution in which the anion ion SO_4^{2-} is stronger than ClO_4^- to chemically adsorb on the Au surface. As shown in Figure S5, the occurrence potential of δ_{AuOH} in Na_2SO_4 is delayed to ~0.45 V and the Raman intensity decreased as well. Explicitly, we infer that the competitive adsorption between hydroxyl and sulfate ions inhibits the onset of hydroxide formation.

To further investigate the effect of crystallographic orientation, comparative experiments were conducted at three low-index Au(*hkl*) single crystal surfaces—Au(111), Au(100), and Au(110)—under identical condition (all electrolytes were deaerated 0.1 M $NaClO_4$ with a pH value of ~9). Evidently, the peak at 790 cm^{-1} features the existence of the intermediate AuOH species, and that peak is chosen to analyze the electrooxidation process on different single crystal surfaces.

Figure 4 displays the intensities of bending mode δ_{AuOH} on three single crystal surfaces increasing in the order of Au(111)

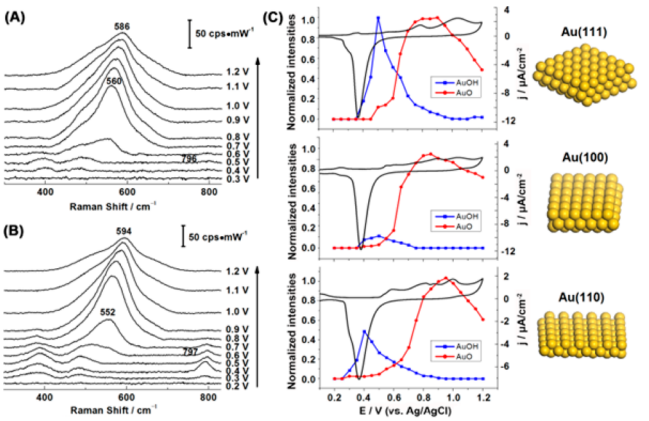

Figure 4. (A,B) EC-SHINERS spectra of electrooxidation of Au(100) and Au(110) surfaces in 0.1 M $NaClO_4$ (pH is ~9). (C) EC-SHINERS intensities of the stretching mode of AuO and the bending mode of AuOH at three low-index Au(*hkl*) surfaces are all scaled to the same maximum value. The corresponding CVs (scan rate is 2 mV/s) are presented as well.

> Au(110) ≫ Au(100), which is consistent with the case of facet-dependent reduction processes presented in Figure S3. The distinct data from our experiments suggest that the energetic favorable formation of hydroxide film on the Au(111) surface occurs through one-electron oxidation of OH^- ions. On the other hand, the intensity of bending mode δ_{AuOH} increases in the order which is in contrast to the activities of the above three gold surfaces in the oxygen reduction reaction (the reaction activity sequence is Au(100) ≫ Au(110) > Au(111)).[20] In essence, we suppose the formation of hydroxide ions during the reduction of the gold surface may retard the oxygen reduction reaction. A detailed mechanism study of this process is currently underway in our group.

In conclusion, in situ EC-SHINERS, along with the crystallographic orientation, pH, and anion effects, was used to systematically characterize and monitor the electrooxidation process on gold single crystal electrodes. The direct observation

DOI: 10.1021/jacs.5b04670
J. Am. Chem. Soc. XXXX, XXX, XXX−XXX

of the chemical nature of the intermediate, AuOH/AuO species, is achieved with the combination of EC-SHINERS and theoretical modeling. This technique will be further applied to examine electrocatalytic processes at noble metal single crystal surfaces to pave a way for technological innovations in energy materials.

■ ASSOCIATED CONTENT

Supporting Information

Experimental section, computational details, deuterium isotopic substitution measurement, EC-SHINERS spectra of Au(*hkl*) electrooxidation and -reduction in 0.1 M $NaClO_4$ and Na_2SO_4. The Supporting Information is available free of charge on the ACS Publications website at DOI: 10.1021/jacs.5b04670.

■ AUTHOR INFORMATION

Corresponding Author

Li@xmu.edu.cn

Author Contributions

#C.-Y.L. and J.-C.D. contributed equally.

Notes

The authors declare no competing financial interest.

■ ACKNOWLEDGMENTS

We thank Z.Y. Zhou for helpful discussion. This research was supported by Thousand Youth Talents Plan of China, the MOST of China (2010IM040100), the Swiss National Science Foundation (200020-144471, and 200021-124643).

■ REFERENCES

(1) (a) Burke, L. D.; Nugent, P. F. *Gold Bull.* **1998**, *31*, 39. (b) Osawa, M. *Bull. Chem. Soc. Jpn.* **1997**, *70*, 2861. (c) Avramov-Ivić, M.; Jovanović, V.; Vlajnić, G.; Popić, J. *J. Electroanal. Chem.* **1997**, *423*, 119. (d) Štrbac, S.; Adžić, R. R. *J. Electroanal. Chem.* **1996**, *403*, 169. (e) Hughes, M. D.; Xu, Y. J.; Jenkins, P.; McMorn, P.; Landon, P.; Enache, D. I.; Carley, A. F.; Attard, G. A.; Hutchings, G. J.; King, F.; Stitt, E. H.; Johnston, P.; Griffin, K.; Kiely, C. J. *Nature* **2005**, *437*, 1132. (f) Marković, N. M.; Ross, P. N., Jr. *Surf. Sci. Rep.* **2002**, *45*, 117. (g) Björling, A.; Herrero, E.; Feliu, J. M. *J. Phys. Chem. C* **2011**, *115*, 15509. (h) Wang, D.; Wan, L. J. *J. Phys. Chem. C* **2007**, *111*, 16109.

(2) Conway, B. E. *Prog. Surf. Sci.* **1995**, *49*, 331.

(3) Attard, G. A.; Brew, A.; Ye, J. Y.; Morgan, D.; Sun, S. G. *ChemPhysChem* **2014**, *15*, 2044.

(4) Angerstein-Kozlowska, H.; Conway, B. E.; Hamelin, A. *J. Electroanal. Chem. Interfac.* **1990**, *277*, 233.

(5) Nguyen Van Huong, G.; Hinnen, C.; Lecoeur, J. *J. Electroanal. Chem. Interfac.* **1980**, *106*, 185.

(6) (a) Shubina, T. E.; Hartnig, C.; Koper, M. T. M. *Phys. Chem. Chem. Phys.* **2004**, *6*, 4215. (b) Dickinson, T.; Povey, A. F.; Sherwood, P. M. A. *J. Chem. Soc. Faraday Trans.* **1975**, *71*, 298. (c) Vassilev, P.; Koper, M. T. M. *J. Phys. Chem. C* **2007**, *111*, 2607. (d) Pessoa, A. M.; Fajín, J. L. C.; Gomes, J. R. B.; Cordeiro, M. N. D. S. *J. Mol. Struct.:THEOCHEM* **2010**, *946*, 43. (e) Adžić, R. R.; Marković, N. M. *J. Electroanal. Chem. Interfac* **1982**, *138*, 443. (f) Koper, M. T. M.; van Santen, R. A. *J. Electroanal. Chem.* **1999**, *472*, 126.

(7) Chen, A.; Lipkowski, J. *J. Phys. Chem. B* **1999**, *103*, 682.

(8) (a) Fleischmann, M.; Hendra, P. J.; McQuillan, A. J. *Chem. Phys. Lett.* **1974**, *26*, 163. (b) Jeanmaire, D. L.; Van Duyne, R. P. *J. Electroanal. Chem. Interfac.* **1977**, *84*, 1. (c) Tian, Z. Q.; Ren, B.; Wu, D. Y. *J. Phys. Chem. B* **2002**, *106*, 9463. (d) McCreery, R. L. *Raman Spectroscopy for Chemical Analysis*; John Wiley & Sons: 2005.

(9) (a) Zou, S.; Weaver, M. J. *J. Phys. Chem.* **1996**, *100*, 4237. (b) Huang, Y. F.; Wu, D. Y.; Wang, A.; Ren, B.; Rondinini, S.; Tian, Z. Q.; Amatore, C. *J. Am. Chem. Soc.* **2010**, *132*, 17199. (c) Li, L.; Steiner, U.; Mahajan, S. *Nano Lett.* **2014**, *14*, 495.

(10) (a) Zheng, J.; Jiao, A.; Yang, R.; Li, H.; Li, J.; Shi, M.; Ma, C.; Jiang, Y.; Deng, L.; Tan, W. *J. Am. Chem. Soc.* **2012**, *134*, 19957. (b) Guerrini, L.; Krpetić, Ž.; van Lierop, D.; Alvarez-Puebla, R. A.; Graham, D. *Angew. Chem., Int. Ed.* **2015**, *54*, 1144.

(11) (a) Abdelsalam, M. E.; Mahajan, S.; Bartlett, P. N.; Baumberg, J. J.; Russell, A. E. *J. Am. Chem. Soc.* **2007**, *129*, 7399. (b) Hu, J.; Tanabe, M.; Sato, J.; Uosaki, K.; Ikeda, K. *J. Am. Chem. Soc.* **2014**, *136*, 10299.

(12) (a) Kim, J.; Gewirth, A. A. *J. Phys. Chem. B* **2006**, *110*, 2565. (b) Zhang, Y.; Gao, X.; Weaver, M. J. *J. Phys. Chem.* **1993**, *97*, 8656. (c) Desilvestro, J.; Weaver, M. J. *J. Electroanal. Chem. Interface* **1986**, *209*, 377. (d) Li, X.; Gewirth, A. A. *J. Am. Chem. Soc.* **2003**, *125*, 7086.

(13) (a) Ren, B.; Picardi, G.; Pettinger, B.; Schuster, R.; Ertl, G. *Angew. Chem., Int. Ed.* **2005**, *44*, 139. (b) Schmid, T.; Opilik, L.; Blum, C.; Zenobi, R. *Angew. Chem., Int. Ed.* **2013**, *52*, 5940.

(14) Bruckbauer, A.; Otto, A. *J. Raman Spectrosc.* **1998**, *29*, 665.

(15) Li, J. F.; Huang, Y. F.; Ding, Y.; Yang, Z. L.; Li, S. B.; Fan, F. R.; Zhang, W.; Zhou, Z. Y.; Wang, Z.; Tian, Z. Q. *Nature* **2010**, *464*, 392.

(16) (a) Li, J. F.; Rudnev, A.; Fu, Y.; Bodappa, N.; Wandlowski, T. *ACS Nano* **2013**, *7*, 8940. (b) Li, J. F.; Ding, S. Y.; Yang, Z. L.; Bai, M. L.; Anema, J. R.; Wang, X.; Wang, A.; Wu, D. Y.; Ren, B.; Hou, S. M.; Wandlowski, T.; Tian, Z. Q. *J. Am. Chem. Soc.* **2011**, *133*, 15922. (c) Honesty, N. R.; Gewirth, A. A. *J. Raman Spectrosc.* **2012**, *43*, 46. (d) Butcher, D. P.; Boulos, S. P.; Murphy, C. J.; Ambrosio, R. C.; Gewirth, A. A. *J. Phys. Chem. C* **2012**, *116*, 5128.

(17) Strbac, S.; Hamelin, A.; Adzić, R. R. *J. Electroanal. Chem.* **1993**, *362*, 47.

(18) Bublitz, G. U.; Boxer, S. G. *Annu. Rev. Phys. Chem.* **1997**, *48*, 213.

(19) Angerstein-Kozlowska, H.; Conway, B. E.; Barnett, B.; Mozota, J. *J. Electroanal. Chem. Interface* **1979**, *100*, 417.

(20) Schmidt, T. J.; Stamenkovic, V.; Arenz, M.; Markovic, N. M.; Ross, P. N., Jr. *Electrochim. Acta* **2002**, *47*, 3765.

DOI: 10.1021/jacs.5b04670
J. Am. Chem. Soc. XXXX, XXX, XXX−XXX